A Multi-Functional Module-Based Capsule Robot

Lingling Zheng, *Student Member, IEEE,* Shuxiang Guo, *Fellow, IEEE*, Zixu Wang, and Takashi Tamiya

***Abstract*—This paper proposes a main-functional module working concept for capsule robots, and the capsule robots consist of a main module and functional modules based on this concept. The main module drives the functional modules and provides guidance and support for the functional modules while the functional modules perform the specific diagnosis or treatment. In addition, we propose a novel single-function design concept, which enables different functional modules to have different functions according to the medical requirements. The diagnosis and treatment functions are separated, and they will allow each module to work more specifically and efficiently. Various functional modules can be selected according to medical requirements, and thus it can improve treatment efficiency and reduce medical costs. The single-function design concept eliminates the need to integrate multiple functions into one robot and decrease manufacturing difficulty. Besides, we present a novel docking-separation method to realize effective docking and rapid separation for capsule robots. It can also enable the docked robot to work in bent parts of intestinal tracts easily. A multimodule capsule robot (MCR) was fabricated and the performance was evaluated through experiments. Experimental results demonstrated that the robot modules could be controlled independently and could dock reliably and separate easily. Moreover, the MCR can prevent accidental separation and has potential applications in the clinical practices of intestinal tracts.**

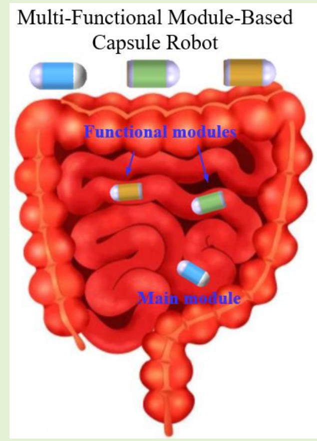

***Index Terms*—Capsule robot, intestinal endoscopy, main-functional module, magnetic navigation.**

I. Introduction

INTESTINAL cancer becomes one of the most common cancers and causes of cancer-associated deaths [1]. Earlier-stage diagnosis and treatments for intestinal diseases can reduce the difficulty of the operation and decrease the fatality rate [2]. Intestinal endoscopy, which uses a long flexible tube with a light and camera to insert from the mouth or anus to the nidus, is used to perform diagnosis and treatments. However, conventional intestinal endoscopy has caused discomfort and pain to patients and some potential complications in the process of operation, which may include perforation, infection, bleeding, and so on. In addition, the success rate mainly depends on the experience of surgeons. Therefore, microrobot has been widely investigated due to its potential applications in the clinical practices of intestinal tracts.

M. Sitti *et al.* proposed a capsule robot controlled by a magnetic field [3]. This robot consists of a ring-shaped external magnetic system, a drug release module and a robotic capsule, and can achieve targeted drug delivery. Besides, they also developed a magnetically actuated soft capsule robot, which enables various advanced functions, including biopsy, drug-releasing, drug injection [4]-[5]. S. Liu *et al.* presented a novel magnetic propulsion system to control movements of the endoscopic capsule in the intestinal tract [6]. Simulated experiments were conducted to demonstrate the controllable movement of the capsule under the developed magnetic propulsion system. Moreover, a novel legged capsule robot actuated by magnetic torque was also developed and it can move through the intestinal lumen [7]. J. Abbott *et al.* presented a novel untethered magnetic device, which is actuated with a single rotating permanent magnet, to realize remote control. This method was demonstrated by actuating rotating magnetic devices in a lumen, and it can be used in active capsule endoscopes and magnetic microrobots [8]-[9]. S. Kim *et al.* developed a new capsule robot using active locomotion to achieve targeted drug release and introduced a micro-fluid manipulation technique, which can control the speed and direction of rotation through spiral machines [10]-[11]. A clamper based and motor-driven capsule robot, mainly composed of a clamper-based locomotion mechanism, a telemetry circuit, and a solid-cylinder three-dimensional receiving coil for wireless power induction, was developed to explore the intestinal tract [12]. Experimental results demonstrated that this capsule robot is suitable for use in minimally invasive intestinal exploration. Two types of magnetic helical robots, developed by G. Jang *et al.*, can helically navigate, release drugs to a target area and unclog

Manuscript received Decmber 13, 2020; revised January 16, 2021; accepted January 28, 2021.

This work was supported in part by the National High-Tech Research and Development Program (863 Program) of China under Grant 2015AA043202, and in part by SPS KAKENHI under Grant 15K2120. (*Corresponding author: Shuxiang Guo*)

L. Zheng, S. Guo, and Z. Wang are with the Graduate School of Engineering, Kagawa University, Takamatsu 761-0396, Japan (e-mail: s19d504@stu.kagawa-u.ac.jp; zhenglingling2018@outlook.com; guo.shuxiang@kagawa-u.ac.jp; s18d501@stu.kagawa-u.ac.jp).

S. Guo is also with the Key Laboratory of Convergence Medical Engineering System and Healthcare Technology, Ministry of Industry and Information Technology, Beijing Institute of Technology, Beijing 100081, China.

T. Tamiya is with the Faculty of Medicine, Kagawa University, Takamatsu 761-0396, Japan (e-mail: tamiya@kms.ac.jp).

tubular structures of the human body by using a mechanical drilling motion [13]-[14]. G. Jang *et al.* also proposed another two crawling magnetic robots using flexible legs in [15]-[16]. Moreover, we have developed two types of magnetically actuated microrobots, and experiments indicated that they have a flexible movement in the pipe and could have potential application in intestinal endoscopy [17]-[20].

These related research topics mainly focus on the design and implementation of single capsule robots. However, complicated surgical operations cannot be performed using a single capsule robot because of dimensional constraints, functional constraints, and lack of cooperation [21]. In our previous research [22], we proposed a robot system with dual capsule robots. The two robots can dock and separate with each other by permanent magnets. However, some challenges exist when the permanent magnets are used as the connect components. (1) The reliability of docking and simplicity of separation are two contradictory requirements. The docked robots would be separated accidentally when the connecting force is set to a small value. Improving the magnetic force can keep the docked robot firm but result in that the docked robot cannot be separated easily. This is because the docking force and the separation force are produced by the same permanent magnets and they have the same value. (2) The movement state of docking and separation is not stable. When the two robot modules move close to each other at a uniform speed, they will accelerate and crash together as the magnetic field density increases with the movement. (3) The docked robot cannot work in some bent parts of the intestinal tract. The docked robot has a long length and it will be stuck in a bent intestine. This affects the operation process of diagnosis and treatment, as well as the operation safety. In [23], Z. Nagy *et al.* developed swallowable modular robots, and the modules can be swallowed one at a time and performed inside the intestinal tract by using cylindrical magnets. This approach enables the robot to work in the bent intestine easily (addressed the challenge (3)) but cannot deal with the challenge (1) and (2). Moreover, some surgeries may have special requirements for the propulsive force, the diagnosis, and the treatment of capsule robots. Due to the restricted design space of the narrow intestinal tract, the existing robot, which integrated the driving mechanism and diagnosis (or treatment) components, cannot perform the movement and diagnosis (or treatment) functions simultaneously and effectively, especially for some complicated surgical operations. Besides, integrating multiple functions into one robot not only increases the manufacturing difficulty, but also improves the medical costs.

In this paper, to extend our previous research, a novel working principle is proposed, and a multimodule capsule robot (MCR) is fabricated. The main contributions of this paper are as follows: (1) We introduce a main-functional module working concept into capsule robots. The main module drives the functional modules and provides guidance and support for the functional modules, while the functional modules perform specific diagnoses and treatments. The main module provides guidance by taking the functional modules to the lesions in the intestinal tract. The support includes energy supply for the

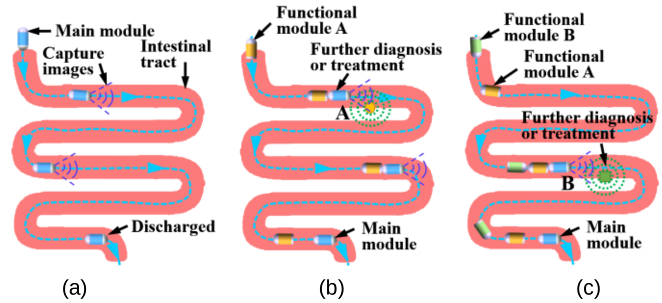

Fig. 1. Schematic diagram of the diagnosis or treatment process of the multimodule capsule robot (MCR): (a) main module; (b) main module and functional module A; (c) main module, functional module A, and functional module B.

functional modules and cooperative actions with the functional modules during procedures, such as biopsy and drug delivery. (2) We propose a novel single-function design concept, which enables different functional modules to have different functions according to the medical requirements. The diagnosis and treatment functions are separated, and they will allow each module to work more specifically and efficiently. Moreover, different functional modules are selected according to medical requirements, and it can improve treatment efficiency and reduce medical costs. The single-function design concept eliminates the need to integrate multiple functions into one robot, and thus it decreases the manufacturing difficulty of capsule robots. (3) A docking-separation method is proposed to realize effective docking and rapid separation of the MCR. It can also enable the docked robot to work in bent parts of the intestinal tract easily.

The remainder of this paper is organized as follows. The principle and design details of the MCR is described in Section II. Section III presents the force and movement analysis, including the propulsive force/torque analysis and kinematic analysis. In Section IV, the performance of the MCR is evaluated and discussed. Finally, the conclusion is given in Section V.

II. Principle and Design

A. Main-Functional Multimodule Type of Capsule Robot

The MCR consists of a main module and functional modules. The main module can dock with functional modules and they can be integrated into a docked robot. The function of the main module is movement control and preliminary diagnosis. It can drive the docked robot and takes it to the lesions in the intestinal tract. Besides, the main module can provide guidance and support for the functional modules, such as energy supply for the functional modules and cooperative actions with the functional modules during procedures. In some difficult surgical operations, such as biopsy and drug delivery, cooperative actions are necessary since great design and manufacturing difficulties exist when a single robot capsule is used. A camera is mounted on the main module, and it can send the position and image information to the robot system. The doctor can complete the preliminary diagnosis based on the image information of the intestinal tract. To enable different functional modules to have different functions according to the medical requirements, we propose a novel single-function design concept. The functional modules have different diagnosis and treatment functions, and each functional module plays a specific therapeutic role. Moreover, when functional modules combine or separate in different forms, they can realize various further therapeutic tasks, such as biopsy and drug release.

Fig. 1 shows the schematic diagram of the diagnosis or treatment process of the MCR. The patient swallows the main module and then the main module moves along the intestinal tract. The camera captures the image of the intestinal tract. If the doctor determines that there is no disease requiring further diagnosis or treatment, the main module moves along the intestine and then is discharged from the anus (Fig. 1 (a)). If further diagnosis or treatment is needed at position A (Fig. 1 (b)), the patient swallows functional module A. Then functional module A docks with the main module. The main module drives the docked robot to position A and performs a further diagnosis or treatment. If a complicated operation is needed at position B (Fig. 1 (c)) and more robot modules are required to achieve cooperative actions, the patient swallows more functional modules (functional modules A and B). Functional modules are driven to position B and docked with the main module. Then the docked robot can perform the complicated operation by using their cooperative actions. After that, all the robot modules are separated from each other and then discharged from the anus.

The main and functional modules can form different states in the intestinal tract. As shown in Fig. 2, the main module links with the functional modules in turn when the MCR is in the "aggregate state"; the main module and the functional modules are separated when the MCR is in the "dispersive state". The type and quantity of functional modules depend on the types of diagnosis and treatment. In addition, the "semi-aggregate state" could also exist, and in this state, some of the robot modules are linked and some are separated.

The main module and functional modules have different structures. As shown in Fig. 3 (a) and (b), the main module is composed of a cover, a main body, and a thread mechanism, while the functional module consists of a claw mechanism, a main body, and a thread mechanism. The claw mechanism and thread mechanism are used to achieve docking and separation. Both main module and functional modules have permanent magnets in their bodies and thus they can be driven by the external magnetic field. In Fig. 3 (c), the main body has two half parts and the magnet is set inside. Moreover, the main module and functional modules have spiral wings on their surfaces. The spiral wings are the driving units of the robot modules and they can provide the power for moving forward or backwards. When a magnetic field is applied to a robot module, the robot module starts to rotate and the driving force is generated with the spiral wings. The force value varies with the change of the spiral wing and the magnetic field. These robot modules move individually in the intestinal tract at first when they are swallowed. Then these robot modules can form different states ("aggregate state", "dispersive state", and "semi-aggregate state") by docking and separation.

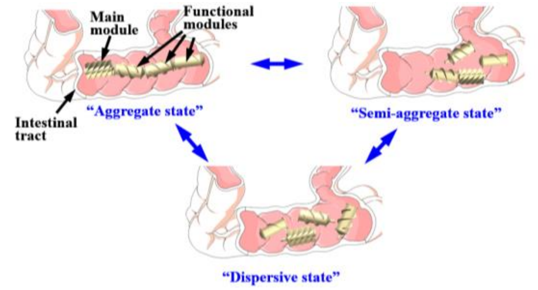

Fig. 2. Schematic diagram of the MCR with different states.

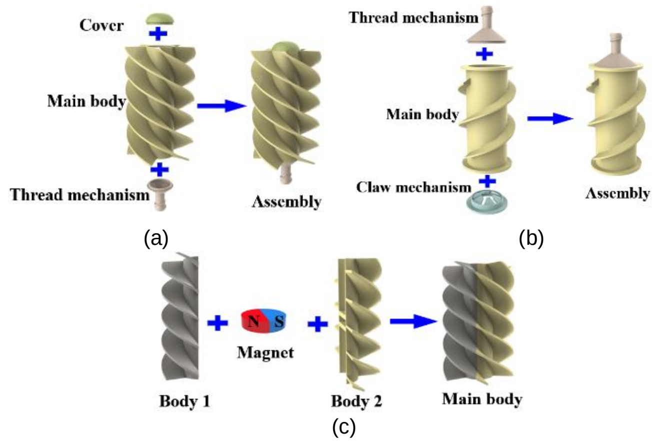

Fig. 3. Structure of the robot: (a) main module; (b) functional module; (c) main body of the main module or functional modules.

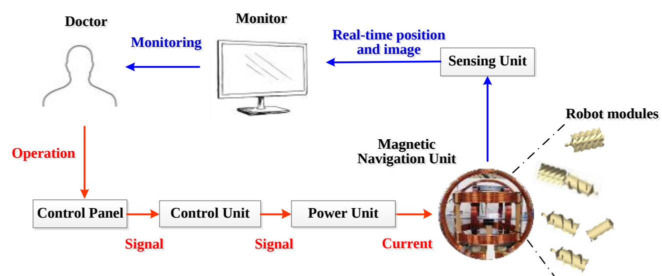

Fig. 4. System overview and control process.

TABLE I
SPECIFICATIONS OF THE MAGNETIC NAVIGATION UNIT

Direction	Diameter (mm)	Coil turns	Wire diameter (mm)	Material	Resistance (Ω)
x	284	125	1	Cu	2.4
y	350	150	1	Cu	3.3
z	400	180	1	Cu	4.5

The system overview and control process are shown in Fig. 4. The doctor manipulates the control panel and the operation information is then sent to the magnetic navigation unit by the control unit and power unit. The magnetic navigation unit is composed of three sets of Helmholtz coils: x-directional Helmholtz coils, y-directional Helmholtz coils, and z-directional Helmholtz coils. The specifications of the magnetic navigation unit are listed in TABLE I. Helmholtz coils are used to generate the magnetic field and thus they can control the movement of the robot. Meanwhile, the sensing unit captures the position and image signals. The doctor can manipulate more accurately and efficiently by using the real-time position and image information.

B. Docking-Separation Method

When the magnetic field is generated, the robot modules will rotate clockwise or counterclockwise and thus it moves forward and backwards. By adjusting the magnitude and direction of the magnetic field, the robot module can reach a target position successfully. When operation requirements exist and two or more robot modules need work cooperatively, the single robot modules dock with each other. As shown in Fig. 2, the main module and functional modules are docked and work as a new docked robot ("aggregate state"), and then swim forward and backwards. The docked robot will separate when the operation is completed (prepare for the next operations or be discharged), and then these robot modules are driven independently. During the process of docking and separation, four challenges exist inevitably. (1) The separation mechanism should enable the docked robot to separate easily while it must be able to prevent the docked robot from separating accidentally. This is the biggest challenge for capsule robots in the process of docking and separation. (2) The docking mechanism should enable robot modules to dock easily. (3) The docked robot can work in some bent parts of the intestinal tract easily. The docked robot has a long length and it will be stuck in a bent intestine. This affects the operation process of diagnosis and treatment, as well as operation safety. (4) The docking method and the separation method should be simple and easy to implement. In addition, due to the size limitation and specificity of magnetic driving mode, the robots need to be controlled without changing existing environmental constraints or adding any extra types of equipment.

In this paper, a novel docking-separation method is proposed and the docking-separation mechanism is shown in Fig. 5. It is composed of a thread mechanism and a claw mechanism. The claw mechanism consists of a sunken base and six claws. Six claws are arranged in a ring shape and a hole is formed at the end of these six claws. The hole has screw threads in it. The thread mechanism consists of a convex base and a rod. A cone is mounted on the other end of the rod. The rod and cone have screw threads on their surfaces. Each functional module has a claw mechanism and a thread mechanism in both ends of their bodies; the main module has a claw mechanism in its tail (Fig. 3 (a) and (b)).

When two robot modules need to dock with each other, the two robot modules swim toward each other (Fig. 6 (a)). With the decrease of the distance, the rod gets into the hole with the assistance of guidance of the sunken base. The rod touches the claws and then the claws move outward as the rod pushes them with the decrease of the distance (Fig. 6 (b)). The rod continues to advance and thus the claws keep moving outward. Finally, the rod enters the hole entirely and the docking task is completed (Fig. 6 (c)). When the docked robot needs to be separated, they rotate in opposite directions. The rod will screw out of the hole with the help of the screw threads both on the rod and the claws (Fig. 6 (d)-(e)). Then these two robot modules separate and swim independently again (Fig. 6 (f)). In this research, the external diameter of robot modules was designed to be smaller than the internal diameter of the intestine. The axes of the two robot modules may not be completely coaxial when they try to dock. However, with the docking-separation

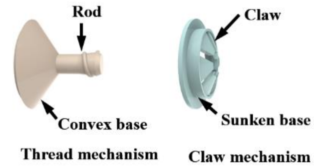

Fig. 5. Docking-separation mechanism.

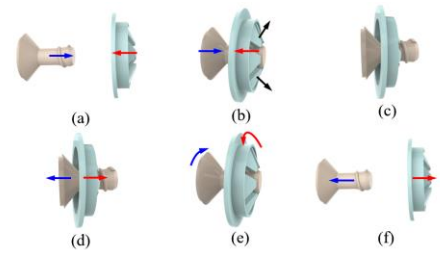

Fig. 6. Motion states of the docking-separation mechanism during the process of docking and separation: (a)-(c) process of docking; (d)-(f) process of separation.

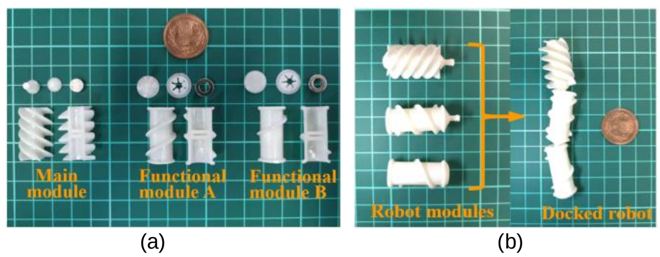

Fig. 7. (a) Components of the MCR; (b) assembled robot modules and docked robot.

method, the robot modules have good fault tolerance for the position of the robot modules before docking since the claws are set obliquely and able to guide the rod to move into the hole. Besides, all the robot modules are designed with different step-out frequency, which enables one robot module to rotate while the other one keeps static or shake slightly in situ when the same magnetic field is applied (discussed in Section IV-A-(2)). By using this characteristic, two robot modules can achieve separation easily.

The docking-separation mechanism has a self-locking feature and it can prevent accidental separation. During the process of docking, the rod can get into the hole easily with the linear movement. However, the rod cannot get out of the hole only by moving forward or backwards because of the self-locking feature. To achieve simple separation, the self-locking can be eliminated by relative rotation of the two robot modules. When the two robot modules rotate in the opposite direction, the rod can get out of the hole by using the screw threads. Moreover, this docking-separation mechanism can enable a docked robot to work in bent parts of the intestinal tract easily, since the thread mechanism and claw mechanism can from an angle and rotate relative to each other like a hinge (analyzed in Section III-B).

C. Design of the Multimodule Capsule Robot

Robot components shown in Fig. 7 (a) were fabricated by 3D printing. These components were assembled into robot modules and these modules can be docked as a docked robot (Fig. 7 (b)). In this paper, one main module and two functional

TABLE II

PARAMETERS OF THE MULTIMODULE CAPSULE ROBOT

Property	Length of the body (mm)	Diameter of the body (mm)	Spiral numbers	Lead angle (°)	Depth of the spiral wings (mm)	Width of the spiral wings (mm)
Main module	36.6	17	5	78.2	4.9	1
Functional module A	36.6	17	2	44.5	2.1	0.6
Functional module B	31.1	17	1	33.7	1.5	0.5

modules, namely functional module A and functional module B, were developed. The design parameters of the MCR with these three robot modules are shown in Table II.

III. MOVEMENT ANALYSIS

A. Propulsive Force/Torque Analysis

When the robot module rotates in the pipe under the external rotating magnetic field, the propulsive force is generated. The spiral wing on the robot module divides the surface into two zones: zone A and zone B. As shown in Fig. 8, zone A (or zone B) can be regarded as a moving body relative to the pipe. Thus, based on the Reynolds equation, the distribution function of fluid pressure in zone A or B can be expressed as

$$\frac{\mathrm{d}p(x,y)}{\mathrm{d}x}=6\mu U\left(\frac{h(x)-\int_0^l \frac{\mathrm{d}x}{h^2(x)} \Big/ \int_0^l \frac{\mathrm{d}x}{h^3(x)}}{h^3(x)}\right) \quad (1)$$

where $p(x,y)$ is the fluid pressure, μ is the dynamic viscosity of the fluid, U is the velocity of zone A (or zone B) relative to the pipe, and $h(x)$ is the edge shape equation of zone A (or zone B). The edge shape equation of zone A (or zone B) can be written as

$$h(x)=\begin{cases} h_{\mathrm{A}} & x\in[0,a) \\ h_{\mathrm{B}} & x\in[a,a+b] \end{cases} \quad (2)$$

where h_{A} is the distance of zone A from the pipe, and h_{B} is the distance of zone B from the pipe. The fluid pressure in zone A and B can be obtained by substituting (2) into (1) and they are as follows:

$$p_{\mathrm{A}}(x,y)=\frac{6\mu U}{h_{\mathrm{A}}^2}\left(1-\frac{h_{\mathrm{A}}^2 h_{\mathrm{B}} b+h_{\mathrm{B}}^3 a}{h_{\mathrm{A}}^3 b+h_{\mathrm{B}}^3 a}\right)x \quad (3)$$

$$\begin{aligned} p_{\mathrm{B}}(x,y)=\frac{6\mu U}{h_{\mathrm{A}}^2}\Big[a\Big(1-\frac{h_{\mathrm{A}}^2 h_{\mathrm{B}} b+h_{\mathrm{B}}^3 a}{h_{\mathrm{A}}^3 b+h_{\mathrm{B}}^3 a}\Big) \\ +\frac{h_{\mathrm{A}}^2}{h_{\mathrm{B}}^2}\Big(1-\frac{h_{\mathrm{A}}^3 b+h_{\mathrm{A}} h_{\mathrm{B}}^2 a}{h_{\mathrm{A}}^3 b+h_{\mathrm{B}}^3 a}\Big)(x-a)\Big] . \end{aligned} \quad (4)$$

The fluid pressure generates normal stress and shearing stress to the robot module. The normal stress and part of the shearing stress work as the motive power for the robot movement while part of the shearing stress works as the resistance for the robot movement. Based on equation (3), the normal stress reaches a maximum value in the edge of the spiral wing. The maximum value can be written as

$$p_{\mathrm{A}}=\frac{6\mu a U}{h_{\mathrm{A}}^2}\left(1-\frac{h_{\mathrm{A}}^2 h_{\mathrm{B}} b+h_{\mathrm{B}}^3 a}{h_{\mathrm{A}}^3 b+h_{\mathrm{B}}^3 a}\right) . \quad (5)$$

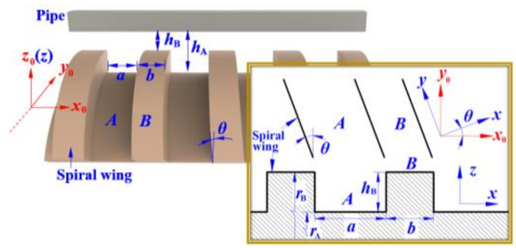

Fig. 8. Schematic diagram for the propulsive force/torque analysis.

The stressed area of the spiral wing can be obtained by

$$S=\pi n h_{\mathrm{A}}(r_{\mathrm{A}}+r_{\mathrm{B}}) \quad (6)$$

where S is the stressed area of the spiral wing, n is the number of the spiral wing, r_{A} is the radius of zone A, and r_{B} is the radius of zone B. Therefore, the motive power generated by the normal stress (F_{ns}) can be obtained by

$$F_{\mathrm{ns}}=p_{\mathrm{A}}S . \quad (7)$$

The fluid in the pipe can be regarded as an incompressible fluid and thus the dynamic viscosity of the fluid is a constant. Based on Navier-Stokes equations, the shearing stress can be obtained by

$$\tau_x=-\frac{h(x)}{2}\frac{\partial p(x,y)}{\partial x}-\frac{\mu}{h(x)}U_x \quad (8)$$

$$\tau_y=-\frac{h(x)}{2}\frac{\partial p(x,y)}{\partial y}-\frac{\mu}{h(x)}U_y \quad (9)$$

where τ_x is the shearing stress in the x-direction, U_x is the velocity of zone A (or zone B) relative to the pipe in the x-direction, τ_y is the shearing stress in the y-direction, and U_y is the velocity of zone A (or zone B) relative to the pipe in the y-direction. The velocity of zone A (or zone B) relative to the pipe is as follows:

$$U_x=v_{\mathrm{r}}\sin\theta-v_{\mathrm{a}}\cos\theta \quad (10)$$

$$U_y=v_{\mathrm{r}}\cos\theta+v_{\mathrm{a}}\sin\theta \quad (11)$$

where v_{r} is the radial velocity of the robot module, θ is the elevation angle of the spiral wing, and v_{a} is the axial velocity of the robot module. The radial velocity of the robot module can be expressed as

$$v_r=\begin{cases} r_{\mathrm{A}}\omega & x\in[0,a) \\ r_{\mathrm{B}}\omega & x\in[a,a+b] \end{cases} \quad (12)$$

where ω is the rotational speed of the robot module.

The force generated by the shearing stress can be obtained by

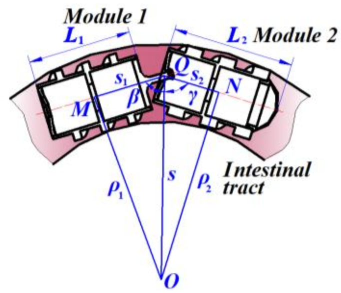

Fig. 9. Kinematic analysis for the docked robot in bent parts of the intestinal tract.

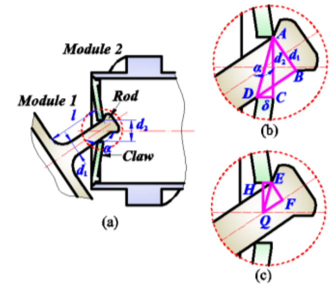

Fig. 10. Kinematic analysis for the docking-separation mechanism: (a) overall diagram; (b)-(c) enlarged diagram.

using integrals and they are as follows:

$$\begin{cases} F_{\mathrm{A}x} = \iint \tau_{\mathrm{A}x} \mathrm{d}x\mathrm{d}y, \ \ F_{\mathrm{A}y} = \iint \tau_{\mathrm{A}y} \mathrm{d}x\mathrm{d}y \\ F_{\mathrm{B}x} = \iint \tau_{\mathrm{B}x} \mathrm{d}x\mathrm{d}y, \ \ F_{\mathrm{B}y} = \iint \tau_{\mathrm{B}y} \mathrm{d}x\mathrm{d}y \end{cases} \tag{13}$$

where $F_{\mathrm{A}x}$ ($F_{\mathrm{A}y}$) is the force generated by the shearing stress in the x-direction (y-direction) in zone A, $\tau_{\mathrm{A}x}$ ($\tau_{\mathrm{A}y}$) is the shearing stress in the x-direction (y-direction) in zone A, $F_{\mathrm{B}x}$ ($F_{\mathrm{B}y}$) is the force generated by the shearing stress in the x-direction (y-direction) in zone B, and $\tau_{\mathrm{B}x}$ ($\tau_{\mathrm{B}y}$) is the shearing stress in the x-direction (y-direction) in zone B.

All these equations above are analyzed in the coordinate system {x, y, z}. In order to express the relationship between these equations and robot motion more intuitively, these equations should be transformed into the coordinate system {x_0, y_0, z_0} (Fig. 8). According to the analysis above, the axial propulsive force of the robot module (F_{ap}) can be expressed as

$$F_{\mathrm{ap}} = F_{\mathrm{ns}} \cos\theta + F_{\mathrm{A}x} \cos\theta + F_{\mathrm{B}x} \cos\theta . \tag{14}$$

The axial resistance of the robot module (F_{ar}) can be expressed as

$$F_{\mathrm{ar}} = F_{\mathrm{A}y} \sin\theta + F_{\mathrm{B}y} \sin\theta . \tag{15}$$

Therefore, the resultant force of the robot module in the axial direction (F_{a}) is

$$F_{\mathrm{a}} = F_{\mathrm{ap}} + F_{\mathrm{ar}} . \tag{16}$$

Similarly, the resultant force of the robot module in the radial direction (F_{r}) is

$$F_{\mathrm{r}} = F_{\mathrm{ns}} \sin\theta + F_{\mathrm{A}y} \cos\theta + F_{\mathrm{B}y} \cos\theta . \tag{17}$$

Therefore, the resultant torque of the robot module (T) can be obtained by

$$T = \left(\frac{r_{\mathrm{A}} + r_{\mathrm{B}}}{2}\right) F_{\mathrm{r}} . \tag{18}$$

The propulsive force and torque of the robot module can be calculated by equations (16) and (18). When the robot module achieves a balance of motion (i.e., uniform motion or rotation), the resultant force or torque of the robot module equals 0. Then the maximal viscosity and rotational speed of the robot module can also be calculated by these equations.

B. Kinematic Analysis

When the docked robot tries to pass through bent parts of intestinal tracts, the axes of every two modules intersect each other and thus the docked robot can move smoothly (shown in Fig. 9, module 1 or 2 can be the main module or functional module A, B…). As shown in Fig. 10 (a), the claw mechanism and thread mechanism form a special pose during the process. The intestinal tract with the smallest radius of curvature that the docked robot can pass through exists when the angle between the axes of two modules reaches the minimum value. In Fig. 9, according to trigonometric function relation, there are

$$\cos\beta = \frac{s_1}{s}, \ \cos\gamma = \frac{s_2}{s} \tag{19}$$

where β is the angle between the axis of module 1 and line segment OQ, point O is the center of gyration of the intestinal tract, point Q is the center of gyration of the docking-separation mechanism, s_1 is the distance of the center of module 1 (point M) from point Q, s is the distance of point O from point Q, γ is the angle between the axis of module 2 and line segment OQ, s_2 is the distance of the center of module 2 (point N) from point Q. As shown in Fig. 10 (a), α is the minimum angle between the axes of two modules and there is

$$\alpha = \beta + \gamma . \tag{20}$$

Substituting (20) into (19) results in

$$\beta = \arctan\frac{s_1 \cos\alpha - s_2}{s_1 \sin\alpha} \tag{21}$$

s_2 is less than s_1 in our design, therefore the smallest radius of curvature of the intestinal tract is ρ_1 and it can be obtained by

$$\rho_1 = s_1 \tan\beta . \tag{22}$$

When (21) is substituted into (22), (22) can be rewritten as

$$\rho_1 = \frac{s_1 \cos\alpha - s_2}{\sin\alpha} . \tag{23}$$

In Fig. 10 (b), the minimum angle between the axes of two modules can be obtained by

$$\alpha = 180^{\circ} - (\angle \mathrm{ADC} - \angle \mathrm{ADB}) \tag{24}$$

where point A, C and D are the points at the end of the claws, point A and B are the transitions point at the change of diameter in the rod. In triangle ADC and triangle ADB, $\angle\mathrm{ADC}$ and $\angle\mathrm{ADB}$ can be expressed as

$$\angle \mathrm{ADC} = \arctan\frac{d_2}{\delta} \tag{25}$$

$$\angle \mathrm{ADB} = \arcsin \frac{d_1}{\sqrt{d_2^2 + \delta^2}} \tag{26}$$

where d_2 is the diameter of the hole formed by the end of six claws, δ is the thickness of the claws, d_1 is the diameter of the rod. When (25) and (26) are substituted into (24), the minimum angle between the axes of two modules can be written as

$$\alpha = 180^{\circ} - \arctan \frac{d_2}{\delta} + \arcsin \frac{d_1}{\sqrt{d_2^2 + \delta^2}}. \tag{27}$$

As shown in (23), the smallest radius of curvature of the intestinal tract that the docked robot can pass through depends on α, s_1 and s_2. According to Fig. 9 and Fig. 10 (c), s_1 and s_2 can be obtained by

$$s_1 = \frac{1}{2} L_1 + l - l_{\mathrm{QF}} \tag{28}$$

$$s_2 = \frac{1}{2} L_2 \tag{29}$$

where L_1 is the length of module 1, l is the length of the rod (excluding the cone), l_{QF} is the length of the line segment QF, and L_2 is the length of module 2. Point Q locates in the center of the hole formed by the end of six claws as it is the center of gyration of the docking-separation mechanism. According to the geometry relationship of triangle EFQ and triangle HEQ, the length of line segment QF and QE can be expressed by

$$l_{\mathrm{QF}} = \sqrt{l_{QE}^2 - \tfrac{1}{4} d_1^2} \tag{30}$$

$$l_{QE}^2 = \frac{1}{4} d_2^2 + \frac{1}{4} \delta^2. \tag{31}$$

Substituting (30) and (31) into (28) results in

$$s_1 = \frac{1}{2} L_1 + l - \frac{1}{2} \sqrt{d_2^2 + \delta^2 - d_1^2}. \tag{32}$$

Therefore, the minimal radius of curvature of the intestinal tract, which the docked robot can pass through smoothly, can be obtained by substituting (27), (29), and (32) into (23). The length of the robot module, the geometry size of the claws and rod affect the radius of curvature of the intestinal tract. The value of the radius can be freely selected by using the proposed method and thus the docked robot can pass through some bent parts of the intestinal tract.

IV. Performance Validation

A. Independent Movement of Robot Modules

1) Experimental Setup

In order to test the feasibility of independent control for every robot module, a main module and two functional modules were used and set in a pipe with liquid. The experimental setup is shown in Fig. 11. The control unit sent out different control signals and then the magnetic navigation unit generated magnetic fields with different frequencies. The robot modules performed different motions with the frequency change of the magnetic fields. The velocities of every module under different frequencies of the magnetic fields were recorded. Moreover, to obtain the motion of robot modules with different directions, different directions of the magnetic fields were adjusted to drive robot modules to move forward and backwards. Each measurement was carried out with ten cycles of repetition.

Fig. 11. Experimental setup for independent movement of the robot modules.

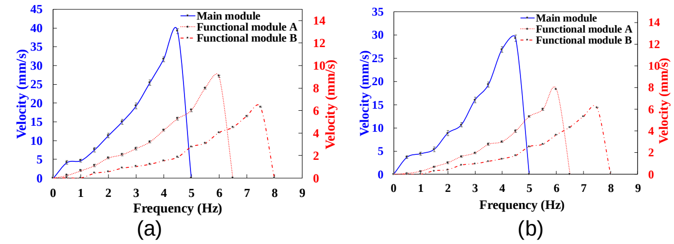

Fig. 12. Experimental results for independent movement: (a) robot modules moving forward; (b) robot modules moving backwards.

2) Experimental Results and Discussion

The velocities of every robot modules when they moved forward and backwards are shown in Fig. 12. The maximal velocity of the main module, functional module A, and functional module B is 39.2 mm/s, 9.1 mm/s, and 6.3 mm/s, respectively, when they moved forward. When they moved backwards, the maximal velocities are 29.3 mm/s, 7.9 mm/s, and 6.2 mm/s.

The experimental results show that each robot module can be controlled by using a magnetic field with different driving frequencies (the robot modules can be driven to move at a frequency, and this frequency is called driving frequency). Thus, a particular driving frequency can be set for every robot module based on the operational requirements. In this experiment, only three modules were selected and tested while the robot could consist of multiple modules. Nevertheless, this experimental setup is acceptable because this principle will still work when more robot modules are used. When more robot modules are needed in operations, the frequency of the magnetic field can be adjusted by changing the geometric and physical parameters of every robot module, such as the moment of inertia, the number of the spiral wing, the lead angle of the spiral wing, and so on.

Robot modules can move from 0 Hz to the step-out frequency (i.e. the robot module stops to move when the driving frequency is larger than this frequency, and this frequency is called step-out frequency). This is mainly because the moment of inertia of the robot module does not match the frequency of the magnetic field. The step-out frequency for every module is 5 Hz, 6.5 Hz and 8 Hz (Fig. 12). The velocities of robot modules were measured by increasing the driving frequency from 0 Hz. The robot modules move extremely

This article has been accepted for publication in a future issue of this journal, but has not been fully edited. Content may change prior to final publication. Citation information: DOI 10.1109/JSEN.2021.3058354, IEEE Sensors Journal

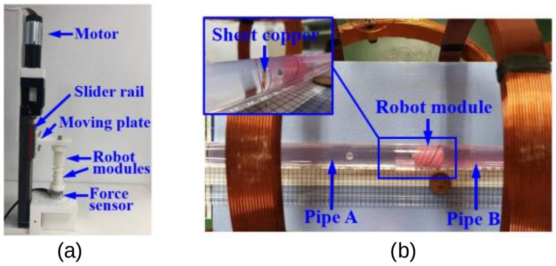

Fig. 13. Experimental setup for force and torque measurement: (a) force and torque required for docking and separation; (b) propulsive force.

slowly at a small driving frequency. The low-speed movement has no practical significance for diagnosis or treatment. Moreover, the robot module cannot keep static entirely because of the peristalsis of the intestinal tract. Therefore, the robot module can be considered static when the velocity is less than 1.5 mm/s. Based on this definition, the range of the driving frequency for the main module, functional module A, and functional module B is 0.5-4.5 Hz, 2.5-6 Hz, and 4-7.5 Hz, respectively.

The real intestine has wrinkles inside, which produce larger friction for the robot modules. The friction would lower the moving speed of the robot modules or even cause the failure of the docking and separation. In the real application, the effect caused by the friction can be reduced effectively by changing with Helmholtz coils with greater magnetic field strength.

B. Docking and Separation

To test whether the robot modules can dock and separate with each other, three experiments were carried out. First, the minimum force/torque required for docking and separation was measured by using a force/torque sensor. Second, experiments were conducted to measure the propulsive force/torque. Finally, docking and separation operations were performed in an in-pipe experiment.

1) Experimental Setup

In the first experiment, one robot module was mounted on a force/torque sensor and the other one was fixed on a plate. The experiment setup is shown in Fig. 13 (a). The moving plate mounted on a slider rail could move up and down. When the slider rail moved toward the force sensor, two robot modules were getting closer until they docked. In this process, the force was captured and the maximum force was the force required for docking operation. This operation was performed ten times. Similarly, we rotated one robot module and let the docked robot achieve the separation. The torque during this process was measured, and the maximum torque was the torque required for separation operation.

In the propulsive force/torque measurement experiment, to measure the propulsive force, a sheet copper was mounted on the connection of two different pipes. As shown in Fig. 13 (b), two pipes (pipe A and pipe B) with liquid, located in the magnetic navigation unit, were connected and used to hold the robot module. When the robot module moved forward, it would push the sheet copper and thus the propulsive force was obtained by calculating the deformation of the copper sheet. To obtain the propulsive torque, an indirect calculation method was designed since the propulsive torque cannot be measured

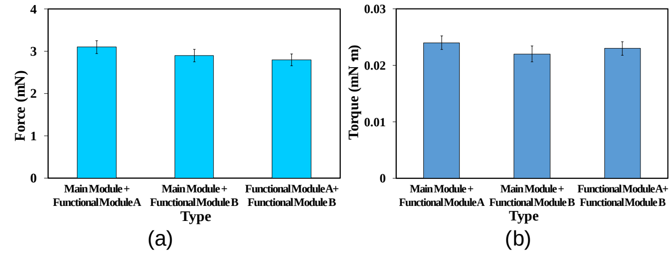

Fig. 14. (a) Required force for docking; (b) required torque for separation.

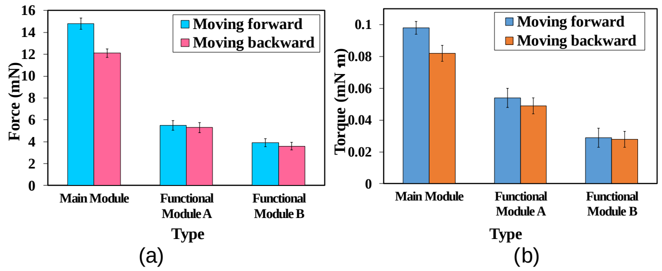

Fig. 15. (a) Propulsive force; (b) propulsive torque.

directly without effect on the movement of the robot module. A camera was used to video the whole moving process of the robot module. During this process, the robot module started to rotate from the static state, then gradually accelerated, and finally rotated at a uniform speed. The rotational speed and time were obtained by the video and thus the propulsive torque was calculated by using this movement information and moment of inertia of the robot module. As the magnetic field is generated by the magnetic navigation unit, the magnetic fields that all the robot modules obtain has the same frequency. Thus, it is difficult to achieve different movements of every robot module at the same time. To obtain the docking and separation of robot modules with the same frequency, the step-out frequency (discussed in Section IV-A-(2)) of every robot module should be within the docking/separation frequency range during docking/separation (the robot modules can be docked/ separated in this frequency range, and this frequency range is called docking/separation frequency range). Therefore, when the main module needs to dock or separate with functional module A, the docking/separation frequency range is set as 3-6 Hz. Similarly, the docking/separation frequency range for the main module and functional module B is set as 4-7.5 Hz; the docking/separation frequency range for functional module A and functional module B is set as 5.5-7.5 Hz. Besides, as robot modules stop to move when the driving frequency is larger than the step-out frequency, the driving frequency range of the main module, functional module A, and functional module B during docking/separation is 3-4.5 Hz, 4-6 Hz, and 5.5-7.5 Hz, respectively. The minimal propulsive forces and torques of every robot module were measured when the driving frequency changed within the above driving frequency ranges. Ten cycles of repetition were carried out for each measurement.

In the third experiment, two robot modules were in a pipe with liquid and they were controlled by the magnetic navigation unit. The two robot modules were driven to move close to and away from each other. At first, they moved close and tried to dock with each other. Then one robot module rotated and tried to separate. Finally, the two modules moved independently.

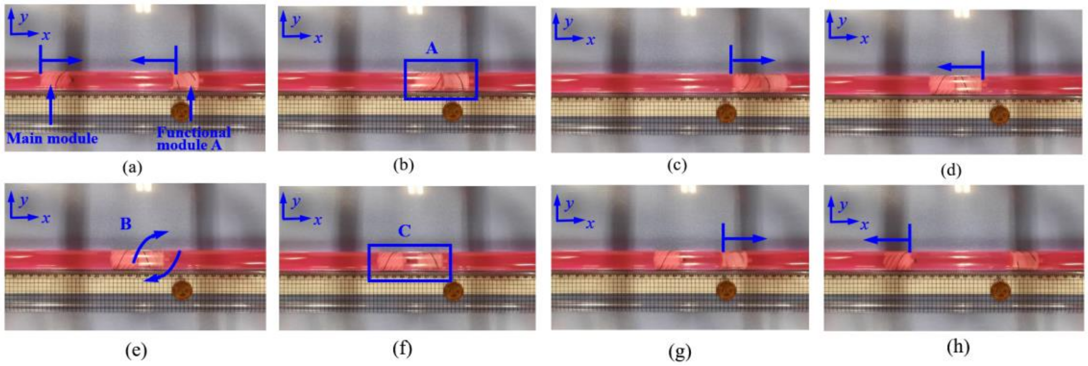

Fig. 16. Video snapshots of the docking and separation procedure: (a) the main module and functional module A rotated and moved towards each other; (b) the main module was docked with functional module A; (c) the docked robot moved forward; (d) the docked robot moved backwards; (e) functional module A started to reverse; (f) the main module was separated from functional module A; (g) functional module A moved forward while the main module remained static; (h) the main module moved backwards while functional module A remained static.

2) *Experimental Results and Discussion*

The required force and torque for docking and separation are shown in Fig. 14. The maximal required force for docking between any two robot modules is 3.1 mN, 2.9 mN, and 2.8 mN, respectively. The maximal required torque for separation between any two robot modules is 0.024 mN·m, 0.022 mN·m, and 0.023 mN·m, respectively. The minimal propulsive force and torque of every robot module within the driving frequency range are shown in Fig. 15. The average minimal propulsive force of the main module, functional module A, and functional module B is 14.8 mN, 5.5 mN, and 3.9 mN, respectively, when they move forward. When they move backwards, the average minimal propulsive forces are 12.1 mN, 5.3 mN, and 3.6 mN, respectively. The minimal propulsive force of every robot module is larger than the maximal required force for docking, and thus any two robot modules can be docked with the propulsive force. The average minimal propulsive torque of the main module, functional module A, and functional module B is 0.098 mN·m, 0.054 mN·m, and 0.029 mN·m, respectively, when they move forward. When they move backwards, the average minimal propulsive torques of the three robot modules are 0.082 mN·m, 0.049 mN·m, and 0.028 mN·m. The minimal propulsive torque of every robot module is larger than the maximal required torque for separation, and thus any two robot modules can be separated with the propulsive torque.

Fig. 16 shows the docking and separation procedure of two robot modules. The main module moved forward and started to dock with functional module A with the decrease of distance. Then the two modules completed the docking task with the propulsive force (position A, Fig. 16 (b)). The docked robot could move forward and backwards (Fig. 16 (c)-(d)). Functional module A reversed and completed the separation task with the propulsive torque (Fig. 16 (e)-(f)). After the separation, the main module and functional module A could move independently. Similarly, two functional modules can also dock and separate from each other. Hence, any two robot modules can be docked and separated successfully by using the proposed docking-separation method.

In this experiment, these two robot modules were positioned in the correct direction, i.e., the thread mechanism of one robot module facing the claw mechanism of the other one, which allows two robot modules to dock or separate just by movement or rotation. In the real environment, the robot modules cannot turn around if they are in the wrong direction since the external diameter of the robot modules was designed to be a little smaller than the internal diameter of the intestine. Therefore, in the real environment, the camera set in the main module should be used to observe the pose of the robot modules and allow robot modules to enter the intestine in correct directions with this navigation.

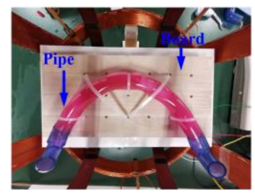

Fig. 17. Experimental setup for movement performance in the bent pipe.

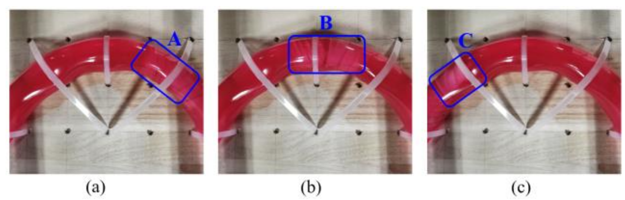

Fig. 18. Video snapshots of the movement procedure in the pipe: (a) the docked robot started to move; (b) the docked robot approached the apex of the pipe; (c) the docked robot passed the apex of the pipe.

C. Movement Performance in Bent Pipes

1) *Experimental Setup*

The docked robot can work in bent parts of the intestinal tract by using the novel docking-separation method. In order to evaluate the movement performance in the bent pipe, a docked robot with two modules was used. It was driven by the magnetic navigation unit and moved in a pipe. The pipe measure 200 mm in the radius of curvature and 25 mm in the internal diameter. The experimental setup is shown in Fig. 17. A board with holes was placed horizontally on the experimental platform and ropes were used to hold the pipe through the holes. The radius of curvature of the pipe can be adjusted by changing the positions of the ropes in the holes. The docked robot moved through the pipe and its movement was captured by a camera.

2) *Experimental Results and Discussion*

The docked robot tried to pass through the bent pipe for ten times and it all passed successfully. The video snapshots of the movement procedure are shown in Fig. 18. The docked robot started to move and the two robot modules formed an angle with the movement (position A). The angle reached the maximal value when it entered the bent parts (position B, Fig. 18 (b)). As Fig. 18 (c) shows, the docked robot finally passed the bent pipe (position C). The proposed robot could consist of several modules while the movement performance of the docked robot with only two modules was tested in this experiment. This is acceptable as the radius of curvature of the docked robot will be same when the number of modules increases. As analyzed in Section III-B, the radius of curvature depends on the geometric parameters of every two docked modules and thus the geometric parameters will be the same when more modules are docked.

D. Accidental Separation Experiment

1) Experimental Setup

When the docked robot moves in the intestinal tract, the force applied to the docked robot can be divided into axial force and radial force. The gastric force is the main force during the operation and it can act as the axial force or radial force for the docked robot. The docking-separation mechanism is more susceptible to external forces in its axial direction. Thus, we tested whether the docked robot can be separated by the gastric force in the axial direction. The experimental setup is the same to that in Fig. 13 (a). We pulled one robot module and made it separate from the other one. The force during this process was recorded and the maximal force was the force that the docked robot can provide to resist separation. Ten cycles of repetition were carried out for each measurement.

In some operational processes, the patient needs to drink some specific liquid. After the liquid is taken, the liquid starts to fall down from the pharynx to the stomach due to the gravity. This type of force mainly affects the docking-separation mechanism in its radial direction and will result in accidental separation of the docked robot. So, in the second experiment, we tested the performance of the docked robot when the water flow acts on the docking-separation mechanism in the radial direction. Fig. 19 shows the experimental setup. A vertical pipe measuring 8 mm in internal diameter, was inserted into a horizontal pipe (24 mm in internal diameter). The docked robot was placed at the junction of the two pipes. The vertical pipe was linked with a pump. The pump can pump water into the pipe and simulate the impact of water flowing on the docked robot. Basically, the patient can drink 400 ml of liquid in 60 seconds (6.67 ml/s) and thus the flow of the pump was set as 8 ml/s (larger than 6.67 ml/s).

2) Experimental Results and Discussion

The maximal force that the docked robot can provide to resist separation was measured. The maximal force is 558$\pm$23mN. [24] declares that the maximal gastric-emptying force is 962.4 dynes/sq cm and thus the maximal force applied to the proposed robot is 30.23mN. This force is far less than the force that the docked robot can provide to resist separation. So the docked robot cannot be separated accidentally with the gastric forces. Besides, the video snapshots during the water impact test are shown in Fig. 20. Driven by the magnetic field, the docked robot shook in situ (stayed at point A) and could not move forward at first as there is no enough water for the docked robot to generate propulsive force (Fig. 20 (a)-(c)). Fig. 20 (b) shows the docked robot suffered from the rush of flowing water and the docked robot remained the original docking state (Fig. 20 (c)). Finally, the docked robot still remained the docking state and moved away when it generated a large propulsive force with the increase of water flow (point B, Fig. 20 (d)). Therefore, the docked robot cannot be separated accidentally when the patient drinks liquid during the procedures.

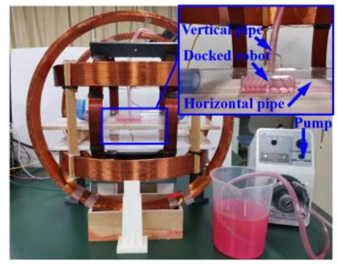

Fig. 19. Experimental setup for the accidental separation experiment.

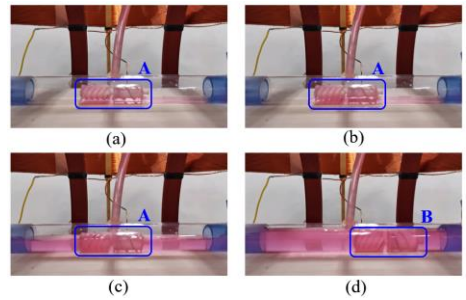

Fig. 20. Video snapshots of the accidental separation experiment: (a) the water started to rush the docked robot; (b) the water flow continued to increase and the docked robot started to rotate; (c) the docked robot remained the docking state; (d) the docked robot moved away in the docking state.

V. Conclusion

In this paper, a main-functional module working concept was introduced and a novel docking-separation method was proposed. Based on the proposed methods, an MCR with three modules was fabricated and evaluated through experiments. The proposed MCR will have the following advantages: (1) Different functional modules can be selected according to medical requirements, and it can improve the treatment efficiency, decrease the manufacturing difficulty, and reduce the medical costs. (2) The main module can provide assistance and perform cooperative actions to some complicated surgical procedures, such as biopsy, drug delivery, or even carry batteries for further treatments. (3) It can dock reliably and separate easily without changing existing environmental constraints or adding any extra types of equipment. (4) The dock robot can work in some bent parts of the intestinal tract successfully. However, some limitations still exist inevitably. The evaluation experiments were conducted in a pipe and the experimental environment differs from that in the real intestinal tract, such as the diameter, the velocity and viscosity of the liquid. More influence factors should be considered in the evaluation experiments. In further research, these limitations will be addressed and in-vivo experiments will be carried out.

REFERENCES

[1] J. Ferlay, I. Soerjomataram, R. Dikshit, S. Eser, C. Mathers, M. Rebelo, D. Parkin, D. Forman, and F. Bray, “Cancer incidence and mortality worldwide: Sources, methods and major patterns in GLOBOCAN 2012,” *Int. J. Cancer*, vol. 136, no. 5, pp. E359-E386, 2014.

[2] D. Keller, A. Windsor, R. Cohen, and M. Chand, “Colorectal cancer in inflammatory bowel disease: review of the evidence” *Tech. Coloproctol*, vol. 23, pp. 3-13, 2019.

[3] F. Munoz, G. Alici, H. Zhou, W. Li, and M. Sitti, “Analysis of magnetic interaction in remotely controlled magnetic devices and its application to a capsule robot for drug delivery,” *IEEE/ASME Trans. Mechatronics*, vol. 23, no. 1, pp. 298-310, 2018.

[4] S. Yim, and M. Sitti, “Design and rolling locomotion of a magnetically actuated soft capsule endoscope”, *IEEE Trans. Robot.*, vol. 28, no. 1, pp. 183-194, 2012.

[5] D. Son, X. Dong, and M. Sitti, “A Simultaneous Calibration Method for Magnetic Robot Localization and Actuation Systems, ” *IEEE Trans. Robot.*, vol. 35, no. 2, pp. 343-352, Apr. 2019.

[6] M. Gao, C. Hu, Z. Chen, H. Zhang, S. Liu, “Design and fabrication of a magnetic propulsion system for self-propelled capsule endoscope,” *IEEE Trans. Biomed. Eng.*, vol. 57, no. 12, pp. 2891-2902, 2010.

[7] Z. Sun, B. Ye, Y. Qiu, X. Cheng, H. Zhang, and S. Liu, “Preliminary study of a legged capsule robot actuated wirelessly by magnetic torque,” *IEEE Trans. Magn.*, vol. 50, no. 8, Aug. 2014.

[8] A. Mahoney, and J. Abbott, “Generating rotating magnetic fields with a single permanent magnet for propulsion of untethered magnetic devices in a lumen,” *IEEE Trans. Robot.*, vol. 30, no. 2, pp. 411-420, 2014.

[9] N. Nelson, and J. Abbott, “Generating two independent rotating magnetic fields with a single magnetic dipole for the propulsion of untethered magnetic devices,” in *Proc. IEEE Int. Conf. Robot. Autom.*, May 2015, pp. 4056-4061.

[10] S. Kim and K. Ishiyama, “Magnetic robot and manipulation for active-locomotion with targeted drug release,” *IEEE/ASME Trans. Mechatronics*, vol. 19, no. 5, pp. 1651-1659, 2014.

[11] D. Ji and S. Kim, “Functional fluid-manipulation using spiral-type magnetic micromachines as micropumps active valves and channel selectors,” *IEEE Access*, vol. 7, pp. 145596-145603, 2019.

[12] J. Gao, and G. Yan, “Design and implementation of a clamper-based and motor-driven capsule robot powered by wireless power transmission,” *IEEE Access*, vol. 7, pp. 138151-138161, 2019.

[13] J. Nam, W. Lee, J. Kim, and G. Jang, “Magnetic helical robot for targeted drug-delivery in tubular environments,” *IEEE/ASME Trans. Mechatronics*, vol. 22, no. 6, pp. 2461-2468, 2017.

[14] G. Jang, S. Jeon, J. Nam, W. Lee, and G. Jang, “A spiral microrobot performing navigating linear and drilling motions by magnetic gradient and rotating uniform magnetic field for applications in unclogging blocked human blood vessels,” *IEEE Trans. Magn.*, vol. 51, no. 11, pp. 1-4, 2015.

[15] B. Jang, J. Nam, W. Lee, and G. Jang “A crawling magnetic robot actuated and steered via oscillatory rotating external magnetic fields in tubular environments,” *IEEE/ASME Trans. Mechatronics*, vol. 22, no. 3, pp. 1465-1472, 2017.

[16] W. Lee, J. Nam, J. Kim, E. Jung, and G. Jang, “Effective locomotion and precise unclogging motion of an untethered flexible-legged magnetic robot for vascular diseases,” *IEEE Trans. Ind. Electron.*, vol. 65, no. 2, pp. 1388-1397, 2018.

[17] Z. Wang, S. Guo, Q. Fu, and J. Guo, “Characteristic evaluation of a magnetic-actuated microrobot in pipe with screw jet motion,” *Microsyst Technol*, vol. 25, no. 2, pp. 719–727, 2019.

[18] Q. Fu, S. Guo, Y. Yamauchi, H. Hirata, and H. Ishihara, “A novel hybrid microrobot using rotational magnetic field for medical applications,” *Biomed. Microdevices*, vol. 17, no. 2, pp. 31-42, 2015.

[19] Q. Fu, S. Zhang, S. Guo, and J. Guo, “Performance evaluation of a magnetically actuated capsule microrobotic system for medical applications,” *Micromachines*, vol. 9, no. 12, pp. 641-656, 2018.

[20] Q. Fu, S. Guo, Q. Huang, H. Hirata, and H. Ishihara, “Development and evaluation of novel magnetic actuated microrobot with spiral motion using electromagnetic actuation system,” *J. Med. Biol. Eng.*, vol. 36, no. 4, pp. 506–514, 2016.

[21] L. Kim, S. Tang, and S. Yoo, “Prototype modular capsule robots for capsule endoscopies,” in *Proc. 13th Int. Conf. Control Autom. Syst.*, Gwangju, Korea, Oct 2013, pp. 350-354.

[22] S. Guo, Q. Yang, L. Bai, and Y. Zhao, “Develop-ment of multiple capsule robots in pipe,” *Micromachines*, vol. 9, no. 6, pp. 259-265, 2018.

[23] Z. Nagy, R. Oung, J. J. Abbott and B. J. Nelson, "Experimental investigation of magnetic self-assembly for swallowable modular robots," in *Proc. IEEE/RSJ Int. Conf. Intell. Robots Syst.*, Nice, 2008, pp. 1915-1920.

[24] B. Laulicht, A. Tripathi, V. Schlageter, P. Kucera, and E. Mathiowitz, “Understanding gastric forces calculated from high-resolution pill tracking,” in *Proc. Natl. Acad. Sci.*, vol. 107, no.18, pp. 8201-8206, 2010.

Lingling Zheng (S’19) received the M.S. degrees in Electrical and Information Engineering from Anhui University of Technology, Anhui, China, in 2018. She is currently working toward the Ph.D. degree in Intelligent Mechanical Systems Engineering, from Kagawa University, Takamatsu, Japan.

Her current research interests include microrobot and medical robots, especially capsule robot systems.

Shuxiang Guo (F’21) received the Ph.D. degree in Mechano-informatics and Systems from Nagoya University, Japan, in 1995. He is currently a Full Professor at the Department of Intelligent Mechanical Systems Engineering, Faculty of Engineering, Kagawa University, Japan. He is also a chair professor with the Key Laboratory of Convergence Medical Engineering System and Healthcare Technology, The Ministry of Industry and Information Technology, Beijing Institute of Technology, China. He has published about 842 refereed journal and conference papers.

He is the Editor-in-Chief of International Journal of Mechatronics and Automation. His research interests include medical robot systems, microcatheter systems, and biomimetic underwater robots.

Zixu Wang (S’19) received the M.S. degree in Intelligent Mechanical Systems Engineering from Kagawa University, Takamatsu, Japan, in 2018. He is working toward the Ph.D. degree in Intelligent Mechanical Systems Engineering from Kagawa University, Japan.

His current research interests include design, analysis and control of wireless magnetic driven microrobot for biomedical applications.

Takashi Tamiya received the Ph.D. degree from Medical School, Okayama University, Okayama, Japan, in 1990. He had fellowships with Massachusetts General Hospital, Harvard Medical School in the USA from 1993 to 1994. He is currently a Full Professor of Neurological Surgery with the Faculty of Medicine, Kagawa University, Japan.